Journal of Molecular Graphics and Modelling 29 (2011) 906–914

Contents lists available at ScienceDirect

Journal of Molecular Graphics and Modelling

journal homepage: www.elsevier.com/locate/JMGM

Modification of Martini force field for molecular dynamics simulation of hydrophobic charge induction chromatography of lysozyme

Lin Zhang, Shu Bai, Yan Sun*

Department of Biochemical Engineering and Key Laboratory of Systems Bioengineering of the Ministry of Education, School of Chemical Engineering and Technology, Tianjin University, Tianjin 300072, Nankai District, China

ARTICLE INFO

Article history:
Received 14 October 2010
Received in revised form 21 February 2011
Accepted 24 February 2011
Available online 8 March 2011

Keywords:
Martini force field
Modification
Coarse-grained model
All-atom model
Protein adsorption
Desorption

ABSTRACT

Modeling, especially the force field, is crucial for the accuracy of molecular dynamics (MD) simulations. In order for more accurate description of adsorption and desorption behaviors of lysozyme in hydrophobic charge induction chromatography (HCIC), the Martini coarse-grained (CG) force field has been modified based on the statistical analysis and comparison of an all-atom (AA) force field, GROMOS96 43A1, and the Martini force field. The parameters describing the protein–adsorbent interactions have been adjusted to avoid too strong and unrealistic adsorption of lysozyme on the agarose matrix and HCIC ligands. It is found that the adsorption and desorption behaviors monitored using the modified Martini force field and MD simulation are consistent with previous simulation results with 46-bead β-barrel model protein. Repeated adjustment of both protein position and orientation is necessary to generate enough contacts for a stable adsorption. After reducing the pH in the mobile phase, the lysozyme–ligand electrostatic repulsion leads to protein desorption. In the adsorption process, little conformational transition of lysozyme is observed due to its stable structure, which is in line with previous experimental observations. So, it is concluded that after appropriate modification, the Martini force field can be used to examine the HCIC process of lysozyme. The modification strategy has thus extended the applicability of the Martini force field to protein chromatography, and it is expected to facilitate studies of exploring the molecular details in adsorption chromatography of proteins.

1. Introduction

The rapid development of biotechnology industry has facilitated the research and development of purification technology of therapeutic proteins expressed by recombinant DNA technology [1–3]. Hydrophobic charge induction chromatography (HCIC) is one of the new progresses in adsorption chromatography for protein purifications [4]. HCIC is basically a hydrophobic interaction chromatography (HIC), but its ligand is composed of both hydrophobic and ionizable groups, providing both hydrophobic interaction for adsorption and electrostatic repulsion for elution. Therefore, HCIC has many advantages over traditional HIC, such as moderate operation condition, high adsorption capacity, and easy elution of bound proteins. Till now, HCIC has been successfully used in the separation and purification of antibodies [5–12] and various other proteins [7,13–15]. In order for better understanding of HCIC processes for protein separations, fundamental studies have been extensively carried out [10,16–21]. However, it is difficult to explore the molecular details of proteins within adsorbent pores using experimental techniques. For this purpose, molecular dynamics (MD) simulation is a powerful tool to explore the molecular insight into protein adsorption [22–26].

Modeling, especially the force field, is crucial for the accuracy of molecular dynamics simulation. The potential energy and the dynamics process of simulation system are determined by the force field [27]. So, the use of a suitable force field is necessary to get correct simulation results in line with experimental observations. Usually, the functions and parameter sets in a force field are derived from both experimental results and quantum mechanical calculations. In all-atom (AA) force field, parameters are provided for each atom. In coarse-grained (CG) force field, parameters are provided for a bead representing a group of several atoms to decrease the computational cost. In our previous studies [28], CG models of HCIC were constructed and used to provide the molecular insight into protein conformational transition in adsorbent pores, using MD simulation and HPN CG force field. However, the 46-bead β-barrel protein [29] used therein was not a real protein but an ideal model protein. Moreover, MD simulations of hen egg white lysozyme adsorption at a charged solid surface [30–32] and human lysozyme adsorption at a hydrophobic surface [33] have been published recently, using all-atom models. So, we have herein investigated HCIC of lysozyme by using a refined CG model. To

* Corresponding author. Tel.: +86 22 27404981; fax: +86 22 27406590.
E-mail address: ysun@tju.edu.cn (Y. Sun).

1093-3263/$ – see front matter © 2011 Elsevier Inc. All rights reserved.
doi:10.1016/j.jmgm.2011.02.004

do this, the first problem we face is to choose a suitable force field.

Currently, several CG force fields suitable for proteins have been developed, as reviewed in literatures [34–36]. Martini CG force field is one of them, proposed by Marrink et al. [37]. In the force field, an amino acid residue is represented by a number of beads according to a four-to-one mapping. That is, on average, four heavy atoms are simplified to a single bead in the CG model. So, the number of beads for a specific amino acid depends on the molecular structure of the amino acid. This is different from HPN CG force field [29], which uses only one bead to represent an amino acid. Thus, the backbone and side chains can be distinguished in the Martini force field. Meanwhile, four main types of beads are considered in the force field, including polar (P), nonpolar (N), apolar (C), and charged (Q) beads. Furthermore, within a main type, several subtypes are used to denote the hydrogen-bonding capabilities, including donor (d), acceptor (a), and both (da), as well as none (0) or by a number to indicate the degree of polarity (from 1 for lower polarity to 5 for higher polarity). In the Martini force field, the Hamiltonian functions include the bonded energy, the Lennard–Jones (LJ) potential energy, and the Coulomb potential energy. The bonded parameters are determined from the distribution of bond lengths, angles, and dihedrals calculated from the Protein Data Bank (PDB). The parameters for LJ and Coulomb potentials are determined from a comparison between simulation results and experimental measurements of the water/oil partitioning coefficients of the amino acid side-chain analogues. Therefore, the Martini force field is appropriate to construct the CG model of real proteins. It has been successfully used in the simulation of membrane lipids [37], proteins [38], and carbohydrates [39] to explore different biological processes.

Thus, in the present study, we have chosen Martini CG model for the MD simulation studies of the adsorption and desorption of a real protein, lysozyme. However, because of the large deviation of the calculated adsorption behavior from experimental observations, the Martini force field is modified by adjusting the parameters of protein–adsorbent hydrophobic interaction based on an AA force field, GROMOS96 43A1. Then, adsorption and desorption behaviors of lysozyme are monitored by MD simulation using the models.

2. Models and methods

2.1. Simulation systems

The native protein structure used in the present study is constructed from the atomic structure of lysozyme (PDB ID: 3LYZ; Fig. 1a), using the scripts provided by Martini force field (http://md.chem.rug.nl/cgmartini/). The total charge number carried in lysozyme is +8 in adsorption (pH 7.0, contributed by 6 lysine with a charge number of +1 each, LYS1, LYS13, LYS33, LYS96, LYS97, LYS116, 11 arginine with a charge number of +1 each, ARG5, ARG14, ARG21, ARG45, ARG61, ARG68, ARG73, ARG112, ARG125, ARG114, ARG128, 2 glutamic acid with a charge number of −1 each, GLU7, GLU35, and 7 aspartic acid with a charge number of −1 each, ASP18, ASP48, ASP52, ASP66, ASP87, ASP101, ASP119) and +17 in desorption (pH 3.0, contributed by 6 lysine and 11 arginine with a charge number of +1 each).

The HCIC adsorbent is regarded as a planar matrix with immobilized ligands on agarose gel surface. The CG model of ligand is built from the atomic structure of commercial HCIC ligand, 4-mercaptoethyl-pyridine (MEP, Pall Life Sciences, New York, USA), using the protocol described in literature [37]. The structure of ligand model is shown in Fig. 1b. The particle types of beads in the MEP ligand are assigned according to literature [37], as shown in Table 1. The charge number carried in MEP ligand is 0 in adsorption (pH 7.0, use particle type SP1) and +1 in desorption (pH 3.0, use particle type Qd), calculated by its pK_a 4.8. The matrix (agarose) consists of uniformly distributed spherical beads, which is assigned by assuming a hexagonal arrangement [40,41] with a side length of 0.38 nm, as shown in Fig. 1c. According to the atomic structure of agarose (PDB ID: 1AGA) and literature data [37], particle type P5 is assigned for the beads in the matrix. All beads in the matrix are fixed in MD simulations. Thereafter, a CG adsorbent model with ligand density 1.474 μmol/m^2 is constructed by bonding the ligand to the planar matrix, according to the procedure proposed in the previous work [42]. Here, the distribution of bonding sites is set to achieve a uniform coverage.

Table 1
Mapping of MEP ligand in the CG models.

Building block	Particle type
OH–CH_2–CH_2	P2
–CH_2–S–CH_2–	C5
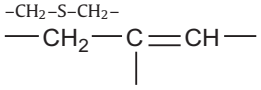	SC4
–CH=N–	SP1/Qd[a]
–CH=CH–	SC4

[a] Particle type is assigned to SP1 in adsorption and Qd in desorption.

To fabricate the simulation system for protein adsorption, a planar adsorbent of size 10.27 nm × 9.88 nm is placed at the bottom of a rectangular water box with a height of 10.00 nm, and a wall of the same size as the adsorbent is placed on the top to keep all beads in the box. The CG water model provided by the Martini force field is used. Then, a native protein is placed over the adsorbent with a distance 1.5 nm (the shortest distance between a residue and a MEP unit or the agarose surface), as shown in Fig. 1c. Six initial orientations of protein with respect to the adsorbent are considered, denoted as O1–O6, as shown in Fig. 1d. Counterions Cl^- are added to ensure the overall neutrality of the system. These are then placed in the center of a cuboid box of size 10.27 nm × 9.88 nm × 50.00 nm for simulation. The simulation system at the end of adsorption is used as the initial configuration for desorption.

2.2. Simulation method

MD simulations in the NVT ensemble are performed to examine the adsorption behaviors of lysozyme, using GROMACS 4.0.5 [43,44] package with the Martini force field [37,38]. A 25 fs time step is used to integrate the equations of motion with the half leap-frog algorithm. The periodic boundary is used in the *x*, *y* and *z* directions. The neighbor list is updated every 10 steps with a cutoff 1.2 nm. The standard shift function of GROMACS is used to deal with the LJ and Coulomb potentials. The LJ potential is shifted from 0.9 nm to a cutoff of 1.0 nm. The Coulomb potential is shifted from 0.0 nm to a cutoff of 1.0 nm. The initial velocities of beads are generated based on the Maxwell distribution at system temperature. The temperature is controlled at 298.15 K by the Berendsen method with a time constant of 0.25 ps.

2.3. Statistical analysis and force field modification

For the modification of Martini force field, atomistic simulations are performed with GROMOS96 43A1 force field. A 2 fs time step is used. The cutoffs of neighbor atom list and LJ potential energy are set to 1.2 and 2.0 nm, respectively. The standard shift function of GROMACS is used to deal with the Coulomb potential, which is shifted from 0.0 nm to a cutoff of 1.0 nm.

A strategy of modification is proposed based on the statistical analysis and comparison of the AA force field and the Martini force field. An AA model of lysozyme is placed in a certain distance *d* away from an AA model of the MEP ligand. It should be

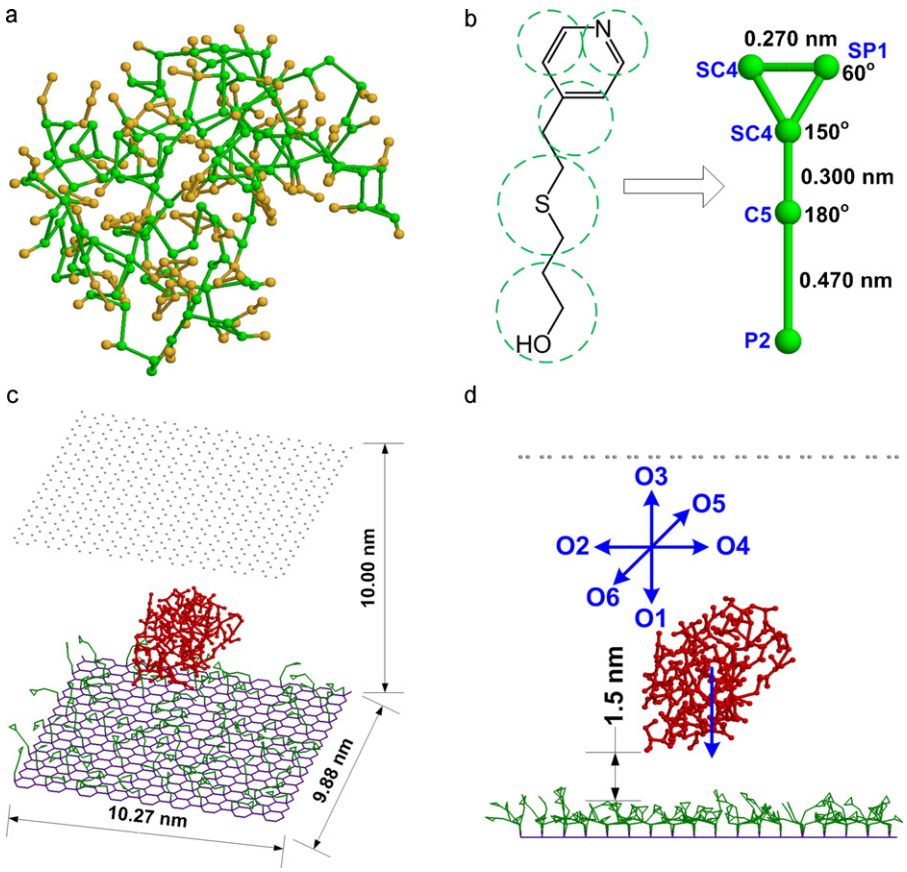

Fig. 1. Coarse-grained models of lysozyme and HCIC adsorbent using Martini force field: (a) native structure of hen egg-white lysozyme; (b) MEP ligand; (c) simulation system; and (d) schematic diagram of initial orientations. In (a), the beads of protein mainchain are drawn in green, and the beads of sidechains are drawn in yellow. In (c) and (d), the beads in lysozyme, MEP ligand, and matrix are drawn in red, green, and purple, respectively. The wall is marked by grey beads.

noted that a lysozyme and a single MEP molecule are used here. The protein–ligand hydrophobic interaction energy (E) is calculated using the AA force field GROMOS96 43A1. Thus, after calculations at various d values, an E–d curve is drawn. With the same procedure, an E–d curve using the Martini force field can be drawn. A minimum of the E–d curve is observed, indicating an interaction equilibrium between these two molecules. The minimum value, E_{min}, indicates the interaction strength. So, for the statistical analysis of the equilibrium energies calculated from the two force fields, 196 pairs of E–d curves are calculated, starting from different initial protein and ligand orientations, and the values of E_{min} are used to calculate the statistical distribution of interaction energies. To get a statistical description, a normal distribution, $N(\mu,\sigma^2)$, is used for the non-linear fitting of the statistical distribution of E_{min}. Finally, the ratio of average interaction energies from the AA and CG models is used for the modification of the parameters related to the protein–adsorbent interaction energy.

2.4. Analysis

Snapshots are prepared using the Rasmol program [45] to describe the microscopic process.

Two parameters are calculated to evaluate the protein conformation: the protein's radius of gyration (R_g) [43,44] and the structural overlap function (χ) [46]. R_g, represents the compactness of the protein conformation, is defined as:

$$R_g = \left(\frac{\sum_i ||\boldsymbol{r}_i||^2 m_i}{\sum_i m_i} \right)^{1/2} \quad (1)$$

where m_i is the mass of atom i and $\boldsymbol{r}_i$ the position of atom i with respect to the center of mass of the molecule. χ, represents the deviation from the native structure of the protein, is defined as:

$$\chi = 1 - \frac{2}{N^2 - 5N + 6} \sum_{i=1}^{N-3} \sum_{j=i+3}^{N} \Theta(\Psi - |r_{ij} - r_{ij}^N|) \quad (2)$$

$$\Theta(x) = \begin{cases} 1 & x \geq 0 \\ 0 & x < 0 \end{cases} \quad (3)$$

where r_{ij}^N is the distance between beads i and j in the native structure, Ψ is the sufferable deviation of the instantaneous configuration from the native structure due to thermal fluctuations, and N is the total number of beads in the model protein.

The adsorption state (B) and desorption state (D) are defined as:

$$\begin{aligned} B &\equiv (d < 0.6) \cap (E_{\text{protein-ligand}} < 0) \quad \text{if lifetime} \geq 0.5 \ \text{ns} \\ D &\equiv B^C \end{aligned} \quad (4)$$

where d is the minimum distance between the protein and ligands, i.e., the shortest distance between a residue and a MEP unit or the agarose surface, and E is the LJ potential energy.

3. Results and discussion

3.1. MD simulation with standard Martini force field

The adsorption of lysozyme is monitored on HCIC adsorbent at a ligand density of 1.474 μmol/m^2, using the CG models constructed by the standard Martini force field. The simulation results show that irreversible adsorption is always observed, regardless of the

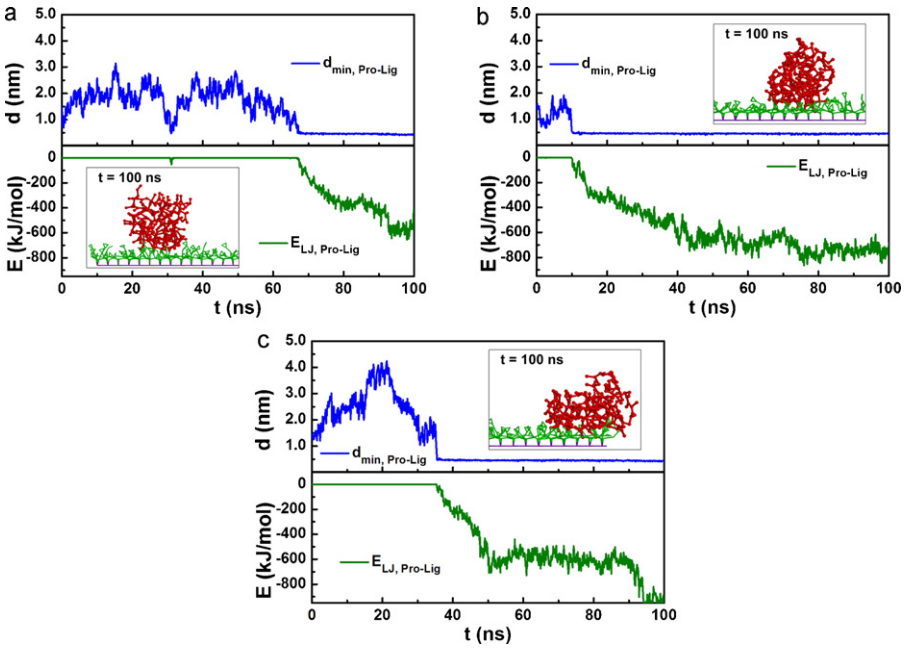

Fig. 2. Typical adsorption trajectories by MD simulations with the Martini force field: (a) O1, (b) O5, and (c) O6. The time courses of *d*, and *E* are shown at the top, and bottom, respectively. The snapshot at the simulation end is provided in the inset.

initial protein orientations considered (i.e., simulations with six initial orientations give consistent results). Three most representative adsorption trajectories, in O1, O5 and O6, are shown in Fig. 2 for more discussion. In O5 (Fig. 2b), the protein keeps at the neighborhood of ligand, and reaches irreversible adsorption quickly, indicating by both the small distance and negative hydrophobic interaction energy between the protein and ligands. Afterward, the protein–ligand distance remains at about 0.47 nm. Meanwhile, the protein–ligand hydrophobic interaction energy decreases slowly, indicating more stable adsorption after the adjustment of protein position and orientation. In O1 (Fig. 2a) and O6 (Fig. 2c), the protein moves away from the ligand surface at first. In O1, however, the protein also keeps at the neighborhood of ligand. At 66.4 ns, the protein becomes adsorbed, followed by a large decrease of the protein–ligand hydrophobic interaction energy. In O6, at 17.5 ns, the protein is 4.1 nm away from the ligand surface, and then keeps free in bulk solution. From 21.3 ns, the protein moves toward the ligand quickly. At 35.3 ns, the protein approaches the ligand, and then is adsorbed immediately. Afterward, the decrease of protein–ligand hydrophobic interaction energy is also observed. From these adsorption trajectories, it can be concluded that regardless of its orientation, once the protein approaches the ligand, it is adsorbed and cannot dissociate from the ligand surface any more. After the protein is adsorbed, the protein–ligand hydrophobic interaction energy continues to decrease. Meanwhile, the protein structure becomes flatter, as indicated by the snapshots (data not shown).

Starting from the stably adsorbed states described above, the desorption behavior at a ligand density of 1.474 μmol/m^2 is monitored, as shown in Fig. 3. Three adsorption trajectories, in O1, O5 and O6, are provided. It can be seen that *d* keeps at a low value in all simulation trajectories. This indicates that the adsorbed protein cannot be disassociated from the ligand surface even after 1000 ns. The protein–ligand interaction energies indicate that hydrophobic attraction is much stronger than electrostatic repulsion. For example, in O3, the protein–ligand LJ potential energy fluctuates around −1000 kJ/mol, while the Coulomb potential energy has a maximum of 12.7 kJ/mol. As shown in formula 2 of reference [38], the Coulomb potential energy is determined by both the charge number and the distance between two charge sites. Herein, the charge number is calculated based on the pK_a of amino acid residues (or MEP ligand), only affected by the pH value. The distance is significant affected by the orientation of protein molecule due to the heterogeneous charge distribution on protein surface (see the blue sites in the snapshots involved in Fig. 3). Therefore, the electrostatic repulsion causes large distance between the beads with both positive charges and thus leads to small electrostatic potential energy. Then, the small Coulomb potential energy is reasonable. That means, not the electrostatic interaction is too weak but the hydrophobic interaction is too strong. The much stronger hydrophobic interaction causes more stable adsorption rather expected desorption.

So, the simulation results in both adsorption and desorption indicate that the adsorption is too strong as compared with both experimental observations and previous simulation results using the HPN CG models [28,42]. For further validation of this problem, the adsorption of lysozyme on the bare matrix, i.e., the agarose matrix without bonding ligands is examined. For comparison with the adsorption on ligand surface (Fig. 2), in this case, the protein trajectories in O1, O5 and O6 are shown in Fig. 4. In the three trajectories, two irreversible adsorptions on the matrix are observed, as shown in O1 (Fig. 4a) and O6 (Fig. 4c), and the energy can reach as low as about −600 kJ/mol (Fig. 4a). Thus, it is confirmed that the Martini force field has provided too strong hydrophobic interactions, which results in protein adsorption on agarose matrix. This is not realistic and never observed experimentally. So, the force field needs modification for its application to protein adsorption to HCIC ligands.

3.2. Modification of lysozyme–adsorbent interaction parameters

Based on the simulation results discussed above, it is confirmed that the model system constructed based on the standard Martini force field has generated too strong and unrealistic adsorption of lysozyme on the HCIC matrix and ligands. So, the parameters in the force field related to the lysozyme–adsorbent hydrophobic interaction should be modified. Recently, an extension of the Martini

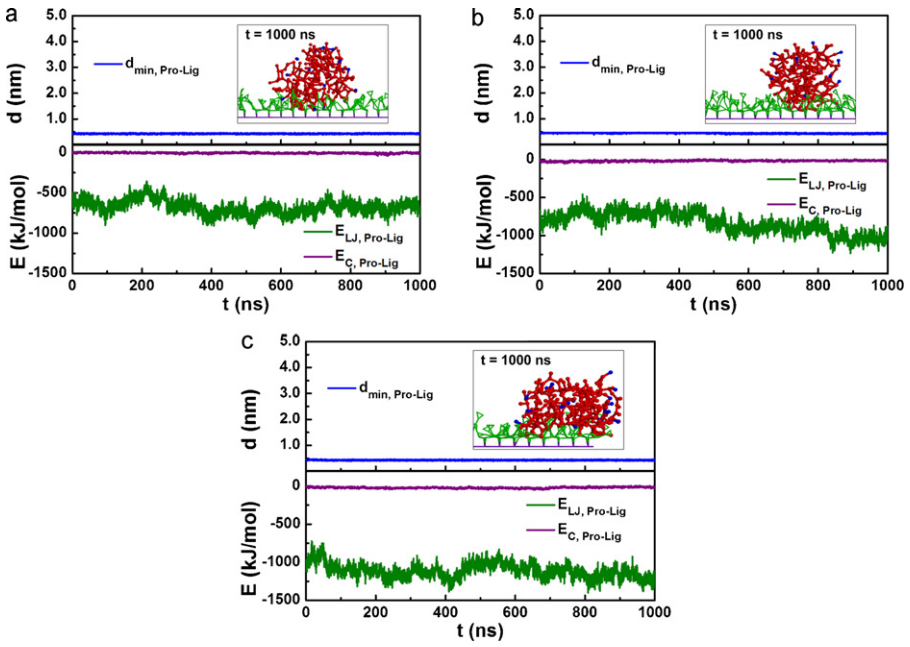

Fig. 3. Typical desorption trajectories by MD simulations with the standard Martini force field, starting from the stably adsorbed states descirbed in Fig. 2: (a) O1, (b) O5, and (c) O6. The time courses of *d*, and *E* are shown at the top, and bottom, respectively. The snapshot at the simulation end is provided in the inset. The beads with positive charge in the protein are marked in blue. (For interpretation of the references to colour in this figure legend, the reader is referred to the web version of this article.)

force field has been performed to simulate collagen molecules, and the parameters are obtained through a combination of experimental and AA simulation data [47]. Here, we have proposed a strategy of modification based on the statistical analysis and comparison of the AA force field and the Martini force field, as described in Section 2.

Examples of the *E*–*d* curves calculated from the GROMOS96 43A1 and the Martini force fields are shown in Fig. 5. It should be noted that a lysozyme and a single MEP molecule are used here. It can be seen that the curves are similar with a standard Lennard–Jones potential energy. Mild attraction is observed as the protein and the ligand approach one another from a distance, and changes to strong repulsion when these two molecules approach too close. A minimum of the *E*–*d* curve is observed, indicating equilibrium between these two molecules. Because the radius of beads in the AA model is different from that in the CG model, a different position of minimum is undoubted and meaningless. However, it is notable the minimum value, E_{min}, indicating the interaction strength, is much different between the two calculations. Namely, the magnitude of the E_{min} from the CG model is much greater than that from the AA model, indicating stronger hydrophobic interaction between the protein and ligand in the CG model.

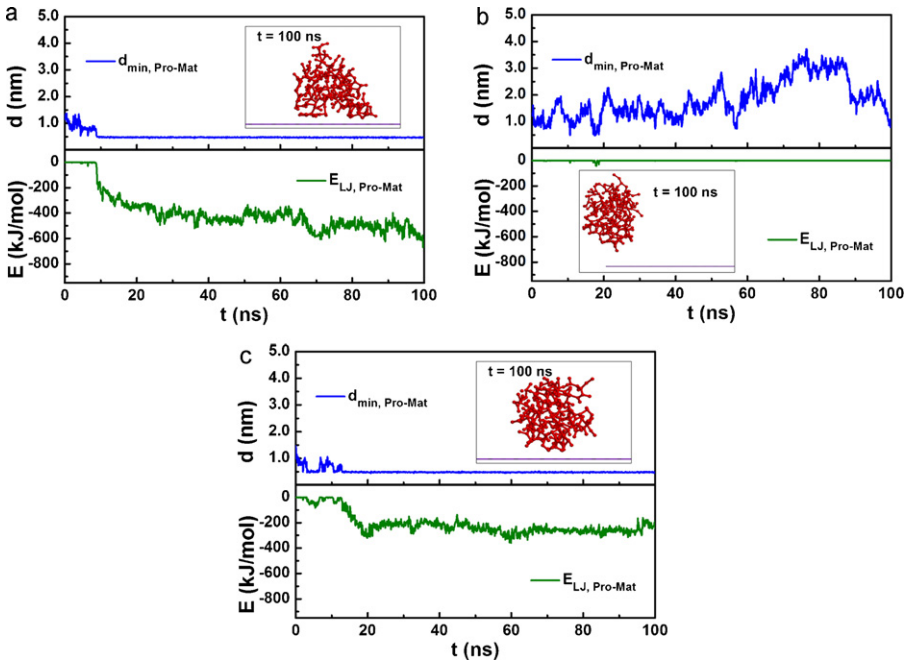

Fig. 4. Typical adsorption trajectories by MD simulations with the Martini force field on the bare agarose matrix: (a) O1, (b) O5, and (c) O6. The time courses of *d*, and *E* are shown at the top, and bottom, respectively. The snapshot at the simulation end is provided in the inset.

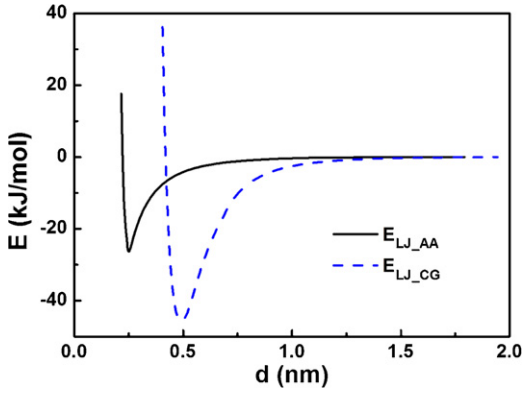

Fig. 5. Potential of mean force of lysozyme–MEP ligand hydrophobic interaction energy with AA force field and CG force field.

This is consistent with the simulation results discussed in Section 3.1. Therefore, the parameters corresponding to the protein–ligand hydrophobic interaction energy in CG model needs to be modified on the basis of the calculations from the AA model.

After calculation of 196 pairs of E–d curves starting from different initial protein and ligand orientations, the statistical distribution of the interaction energies is calculated using the values of E_{min}, as shown in Fig. 6. For the AA model, a range of −50 to 0 kJ/mol is observed, and the most probable distribution locates at −15 to −10 kJ/mol. For the CG model based on the standard Martini force field, a wider range −100 to 0 kJ/mol, is obtained as compared with the AA model, and high distribution probabilities are observed from −40 to −15 kJ/mol. Then, a normal distribution, $N(\mu,\sigma^2)$ is used for the non-linear fitting to get a statistical description. As a result, $N(-14.49,7.44^2)$ and $N(-29.46,14.78^2)$ are obtained for the AA and CG models, respectively. About two times stronger hydrophobic interaction energy in the CG model is confirmed from the statistical analysis. Thus, the parameters in the Martini force field related to the lysozyme–adsorbent hydrophobic interaction is reduced, using the ratio of average interaction energies from the AA and CG models, −14.49/−29.46 = 0.4919. That is, in the modified Martini force field, the parameters related to the protein–adsorbent hydrophobic interaction energy are reduced from 1 to 0.4919. It should be noted that only parameters related to hydrophobic interaction energy is adjusted and the Coulomb potential energy is not affected.

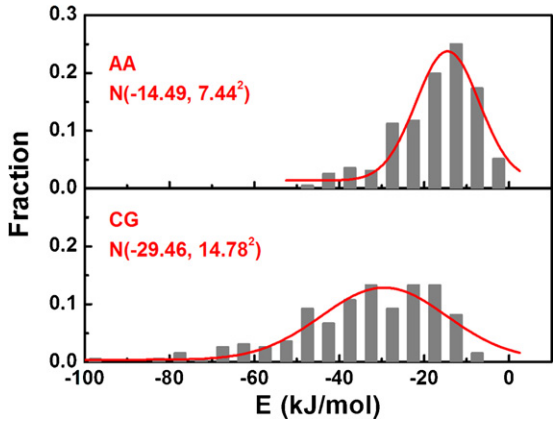

Fig. 6. Distribution of the lysozyme–MEP ligand hydrophobic interaction energies based on AA (top) and CG (bottom) force field. The non-linear fitting using normal distribution $N(\mu,\sigma^2)$ is shown by the red line. The parameters μ and σ^2 are shown in inset. (For interpretation of the references to colour in this figure legend, the reader is referred to the web version of this article.)

3.3. Validation of modified Martini force field

To validate the modified Martini force field, lysozyme adsorption to the bare agarose matrix is first examined. For comparison with Fig. 4, the protein trajectories in O1, O5 and O6 are given in Fig. 7. It can be seen that the protein is always free in the bulk phase, i.e., no stable adsorption can be observed. The protein–adsorbent hydrophobic interaction energy is very weak. Although the protein approaches the matrix several times in O6 (see the green curve in Fig. 7c), the attraction from the matrix cannot maintain the adsorbed state of protein molecule. So, after transitory contact, the protein leaves the matrix and returns to bulk solution. These results indicate that the protein does not bind on the agarose matrix with the modified Martini force field, which is in agreement with experimental observations.

By using the modified Martini force field, lysozyme adsorption on the MEP adsorbent at a ligand density of 1.474 μmol/m^2 is then monitored. Fig. 8a shows the time courses of χ, R_g, the distance between the protein and ligands (d), and the hydrophobic interaction potential energy (E) in O1. Corresponding snapshots marked at different time points in Fig. 8a are shown in Fig. 8b to provide clear description of the adsorption process. As can be seen from the trajectories, at 3.1 ns, the protein moves away from the ligands with hydrophobic interaction energy (green) of zero. Meanwhile, a rapid decrease of R_g is observed, indicating the collapse of protein structure, as a result of different solution condition. The initial lysozyme structure used herein is a crystal structure [48] from PDB. However, the protein is put into aqueous solution to start the simulation. The switch of solution condition causes the rapid adjustment of lysozyme structure. Thereafter, the protein remains free in bulk solution (see the fluctuation of d in Fig. 8a). Rotation and translation of the protein are observed from the snapshots (e.g., snapshot #1 to #2 in Fig. 8b), but no obvious protein conformational transition is observed, indicated by little change of R_g and χ. At 11.8 ns, the protein approaches the ligands and is then transitorily adsorbed, indicated by the low d. After adjustment of the protein position and orientation, another contact takes place around 19.7 ns, indicated by both the low d and negative E. However, this is not a stable adsorption, since a few nanoseconds later, the protein is disassociated and moves in the neighborhood of the ligands. At 30.4 ns, adsorption is observed again. This time, the protein remains on the ligand surface for about 10 ns, and then returns to bulk solution. At 55.5 ns, the protein is far from the ligands. Here, a partially unfolded structure is observed, as shown in snapshot #5 in Fig. 8b. This is also verified by the high value of R_g. But soon, R_g decreases and the protein collapses to a refolded structure. Finally, at 59.0 ns, a stable adsorption is observed. Large decrease of hydrophobic interaction energy (green) indicates the strong attraction of protein molecule. Afterward, the protein–ligand distance, d, remains at a low value (blue), with little fluctuation (for example, at 72.0 ns). The protein–ligand hydrophobic interaction energy, E, continues decreasing (green) and then fluctuates around −50 kJ/mol, indicating the formation of steadily adsorbed state. As compared with the results using standard Martini force field (Fig. 2a), the relevant Martini parameters are reduced by a factor of 0.4919, but E is not reduced to roughly the same extent. In molecular simulation, E is determined by not only the relevant parameters, but also the protein–ligand distance (protein orientation should also be considered). With reduced hydrophobic interaction, the distance is also affected and leads to further reduction of E. Moreover, it can be seen from the snapshots that the protein rotates on the ligand surface, and small conformational transition is also observed to get more stable adsorption (see the red curve in Fig. 8a). So, from the adsorption trajectories, it can be seen that repeated adjustments of both protein position and orientation is necessary to reach a stable adsorption. After being adsorbed, the protein can rotate on

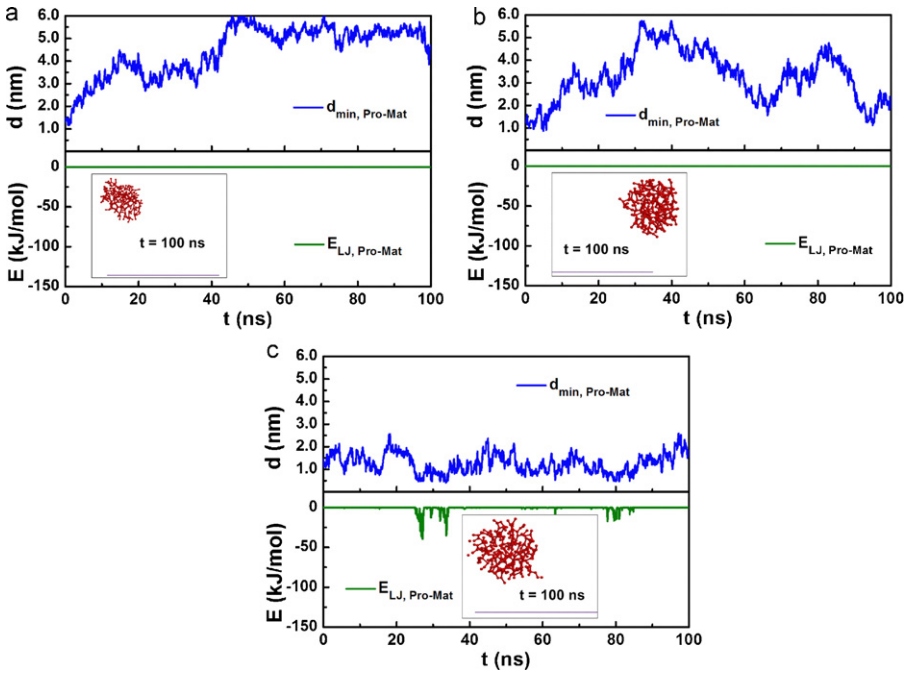

Fig. 7. Typical adsorption trajectories on the bare agarose matrix using the modeified Martini force field: (a) O1, (b) O5, and (c) O6. The time courses of *d*, and *E* are shown at the top, and bottom, respectively. The snapshot at the simulation end is provided in the inset.

the ligand surface to get more stable adsorption. This is in line with the adsorption behavior of 46-bead β-barrel model protein [28]. However, different results are observed on protein conformational transition. In the previous simulation results [28], serious unfolding of 46-bead β-barrel model protein is observed on the ligand surface, which is consistent with the experimental observation for α-lactalbumin adsorption on HIC media [49–51]. Herein, little unfolding of lysozyme is observed in the adsorption process, even on the ligand surface. This is attributed to the stable structure of lysozyme molecule. Experimental studies have confirmed that the stability of lysozyme is not significantly changed during the adsorption in HIC [52]. (For interpretation of the references to colour in this para, the reader is referred to the web version of this article.)

Starting from the adsorbed state at 100 ns in Fig. 8, the charge number carried in lysozyme is changed from +8 (pH 7.0) to +17 (pH 3.0) to monitor the dissociation process, while the charge number carried in MEP ligand is changed from 0 to +1. Here, lysozyme desorption in O1 is provided, using the modified Martini force field, as shown in Fig. 9. The beads in protein with positive charge are shown in blue in the snapshots. At first, the protein keeps in its adsorbed state (see snapshot #1 in Fig. 9b), indicated by both the low *d* and the negative protein–ligands hydrophobic interaction energy. Little conformational transition is observed, as neither R_g nor χ shows significant changes. However, both the protein and ligands are positively charged, leading to electrostatic repulsion. So, the protein is repulsed and disassociated from the ligand surface, indicated by the rapid increase of *d*. In this process,

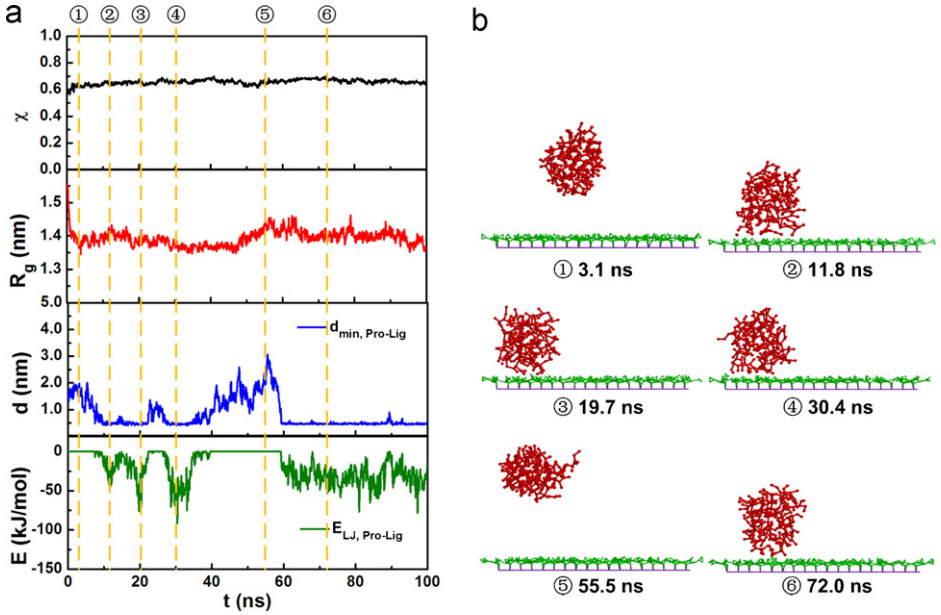

Fig. 8. Adsorption behavior of O1 using the modeified Martini force field. The time courses of χ, R_g, *d* and *E* in adsorption trajectory are shown in (a), and the correspongding snapshots at the time points marked in (a) are shown in (b).

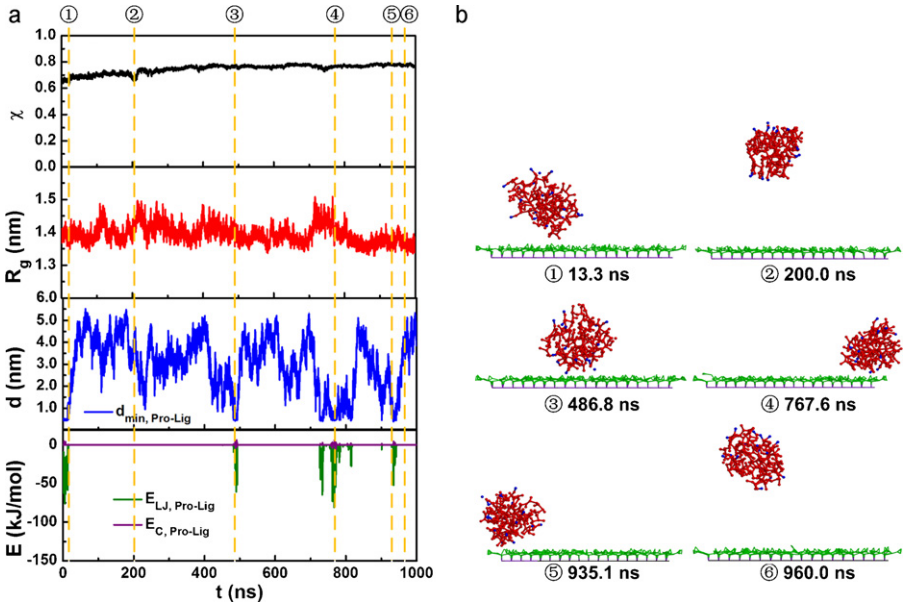

Fig. 9. Desorption behavior of O1 using the modeified Martini force field. The time courses of χ, R_g, d and E in adsorption trajectory are shown in (a), and the correspongding snapshots at the time points marked in (a) are shown in (b). The beads with positive charge in the protein are marked in blue. (For interpretation of the references to colour in this figure legend, the reader is referred to the web version of this article.)

large disturbance of protein conformation is observed, indicated by serious fluctuations on R_g. The χ also continues to increase slowly. An example of the disassociated protein is provided at 200.0 ns (see snapshot #2 in Fig. 9b). At 486.8 ns, the protein approaches the ligands again, but the protein rebounds to the bulk phase quickly, because the beads with positive charges in protein are close to the ligands (see the blue beads in snapshot #3 in Fig. 9b). Thereafter, another two approaches to the ligands are observed at 767.6 and 935.1 ns (see snapshots #4 and #5 in Fig. 9b), but the electrostatic repulsion always prevents the protein from adsorption and keeps it in the free state (see snapshot #6 in Fig. 9b). Therefore, the trajectories and snapshots indicate that the protein can be successfully desorbed in the presence of electrostatic repulsion. As compared with the adsorption process, more distinct unfolding is observed in the desorption process, due to the presence of simultaneous hydrophobic adsorption and electrostatic repulsion in the opposite directions. These results are consistent with previous results with the 46-bead β-barrel model protein [28]. However, the electrostatic repulsion is weaker than that for the 46-bead β-barrel model protein, because lysozyme is much bigger in size and has only a little more positive charges than the model protein.

The 46-bead β-barrel model protein and HPN CG force field [28] can explore the general behaviors of protein in chromatographic process. For example, protein unfolding on the ligand surface can be monitored, which has been verified by extensive experimental results [49–51]. However, the 46-bead β-barrel protein is an ideal model protein with simple structure. For a specific protein, there may be distinct differences. For example, according to the experimental studies [52], the stability of lysozyme is not significantly changed during the adsorption in HIC due to its stable structure, which cannot be described using 46-bead β-barrel model protein. Herein, using the modified Martini force field, the CG model of lysozyme can be constructed, and the adsorption behavior of lysozyme can be described. Moreover, the conformation transition of lysozyme on the ligand surface can be described in line with experimental observations [52]. So, for the molecular simulation of real proteins, the CG models can be constructed using Martini force field. The strategy based on the statistical analysis and comparison of the AA force field and the Martini force field proposed in this work can be carried out to get a more accurate description of simulation system for specific proteins. Then, the adsorption/desorption processes of real proteins can be studied to explored the molecular insight into practical chromatography processes.

4. Conclusions

The Martini CG force field has been utilized to investigate the adsorption and desorption of lysozyme in HCIC using MD simulation. It is shown that the standard Martini force field has generated too strong and unrealistic adsorption of lysozyme on the agarose matrix and HCIC ligands, leading to large deviation from the experimental observations. Then, a strategy of the force field modification is proposed based on the statistical analysis and comparison of the AA force field and the Martini force field, and the parameters describing protein–adsorbent interaction are modified. Using the modified Martini force field, the adsorption and desorption of lysozyme can be described in line with experimental observations and previous simulation results with 46-bead β-barrel model protein. However, the proposed modification is based on simple rescaling of the LJ potential energy. This is a simplistic change that may work on the average, as in this case, but that cannot in general describe accurately specific or local hydrophobic interactions. Meanwhile, different from the serious unfolding of 46-bead β-barrel model protein on the ligand surface, the conformational transition of lysozyme is not obvious in the simulations, which is consistent with experimental studies [52]. Therefore, after reasonable adjustment of the protein–adsorbent interaction parameters, the Martini force field can be applied in HCIC to investigate the adsorption of real proteins. Thus, virtual chromatography experiments using MD simulations with real proteins become realistic. It would be beneficial to the rational design of ligands and parameter optimizations for high-performance HCIC.

Acknowledgments

This work was supported by the Natural Science Foundation of China (Nos. 20636040, 20976126 and 21006069) and the Innovation Foundation of Tianjin University.

References

[1] B. Leader, Q.J. Baca, D.E. Golan, Protein therapeutics: a summary and pharmacological classification, Nat. Rev. Drug Discov. 7 (2008) 21–39.
[2] R. Sodoyer, Expression systems for the production of recombinant pharmaceuticals, Biodrugs 18 (2004) 51–62.
[3] B.K. Nfor, P. Verhaert, L. Van Der Wielen, J. Hubbuch, M. Ottens, Rational and systematic protein purification process development: the next generation, Trends Biotechnol. 27 (2009) 673–679.
[4] S.C. Burton, D.R. Harding, Hydrophobic charge induction chromatography: salt independent protein adsorption and facile elution with aqueous buffers, J. Chromatogr. A 814 (1998) 71–81.
[5] W. Schwartz, D. Judd, M. Wysocki, L. Guerrier, E. Birck-Wilson, E. Boschetti, Comparison of hydrophobic charge induction chromatography with affinity chromatography on protein A for harvest and purification of antibodies, J. Chromatogr. A 908 (2001) 251–263.
[6] M.P. Dux, R. Barent, J. Sinha, M. Gouthro, T. Swanson, A. Barthuli, M. Inan, J.T. Ross, L.A. Smith, T.J. Smith, R. Webb, B. Loveless, I. Henderson, M.M. Meagher, Purification and scale-up of a recombinant heavy chain fragment C of botulinum neurotoxin serotype E in *Pichia pastoris* GS115, Protein Expr. Purif. 45 (2006) 359–367.
[7] G.T. Weatherly, A. Bouvier, D.D. Lydiard, J. Chapline, I. Henderson, J.L. Schrimsher, S.R. Shepard, Initial purification of recombinant botulinum neurotoxin fragments for pharmaceutical production using hydrophobic charge induction chromatography, J. Chromatogr. A 952 (2002) 99–110.
[8] L. Guerrier, P. Girot, W. Schwartz, E. Boschetti, New method for the selective capture of antibodies under physiolgical conditions, Bioseparation 9 (2000) 211–221.
[9] L. Guerrier, I. Flayeux, E. Boschetti, A dual-mode approach to the selective separation of antibodies and their fragments, J. Chromatogr. B 755 (2001) 37–46.
[10] E. Boschetti, Antibody separation by hydrophobic charge induction chromatography, Trends Biotechnol. 20 (2002) 333–337.
[11] H. Bak, O.R. Thomas, Hydrophobic charge induction chromatography for the purification of polyclonal antibodies from clarified rabbit antisera, J. Biotechnol. 131 (2007) S130–S131.
[12] T. Arakawa, Y. Kita, H. Sato, D. Ejima, MEP chromatography of antibody and Fc-fusion protein using aqueous arginine solution, Protein Expr. Purif. 63 (2009) 158–163.
[13] S. Ghose, B. Hubbard, S.M. Cramer, Evaluation and comparison of alternatives to Protein A chromatography – mimetic and hydrophobic charge induction chromatographic stationary phases, J. Chromatogr. A 1122 (2006) 144–152.
[14] D. Coulon, C. Cabanne, V. Fitton, A.M. Noubhani, E. Saint-Christophe, X. Santarelli, Penicillin acylase purification with the aid of hydrophobic charge induction chromatography, J. Chromatogr. B 808 (2004) 111–115.
[15] Y.K. Chang, S.Y. Chou, J.L. Liu, J.C. Tasi, Characterization of BSA adsorption on mixed mode adsorbent – I. Equilibrium study in a well-agitated contactor, Biochem. Eng. J. 35 (2007) 56–65.
[16] G.F. Zhao, G.Y. Peng, F.Q. Li, Q.H. Shi, Y. Sun, 5-Aminoindole, a new ligand for hydrophobic charge induction chromatography, J. Chromatogr. A 1211 (2008) 90–98.
[17] Q.H. Shi, Z. Cheng, Y. Sun, 4-(^{1}H-imidazol-1-yl) aniline: a new ligand of mixed-mode chromatography for antibody purification, J. Chromatogr. A 1216 (2009) 6081–6087.
[18] S. Ghose, B. Hubbard, S.M. Cramer, Protein interactions in hydrophobic charge induction chromatography (HCIC), Biotechnol. Progr. 21 (2005) 498–508.
[19] P. Gagnon, IgG aggregate removal by charged-hydrophobic mixed mode chromatography, Curr. Pharm. Biotechnol. 10 (2009) 434–439.
[20] J. Chen, J. Tetrault, A. Ley, Comparison of standard and new generation hydrophobic interaction chromatography resins in the monoclonal antibody purification process, J. Chromatogr. A 1177 (2008) 272–281.
[21] G.F. Zhao, Y. Sun, Displacement chromatography of proteins on hydrophobic charge induction adsorbent column, J. Chromatogr. A 1165 (2007) 109–115.
[22] L. Zhang, Y. Sun, Molecular simulation of adsorption and its implications to protein chromatography: a review, Biochem. Eng. J. 48 (2009) 408–415.
[23] D. Frenkel, B. Smit, Understanding Molecular Simulation: From Algorithms to Applications, 2nd ed., Academic Press, San Diego, CA, 2002.
[24] A.A. Mungikar, D. Forciniti, Computer simulations and neutron reflectivity of proteins at interfaces, Chemphyschem 3 (2002) 993–999.
[25] G. Raffaini, F. Ganazzoli, Understanding the performance of biomaterials through molecular modeling: crossing the bridge between their intrinsic properties and the surface adsorption of proteins, Macromol. Biosci. 7 (2007) 552–566.
[26] Y. He, J. Hower, S.F. Chen, M.T. Bernards, Y. Chang, S.Y. Jiang, Molecular simulation studies of protein interactions with zwitterionic phosphorylcholine self-assembled monolayers in the presence of water, Langmuir 24 (2008) 10358–10364.
[27] A.D. Mackerell, Empirical force fields for biological macromolecules: overview and issues, J. Comput. Chem. 25 (2004) 1584–1604.
[28] L. Zhang, G.F. Zhao, Y. Sun, Molecular insight into protein conformational transition in hydrophobic charge induction chromatography: a molecular dynamics simulation, J. Phys. Chem. B 113 (2009) 6873–6880.
[29] J.D. Honeycutt, D. Thirumalai, Metastability of the folded states of globular proteins, Proc. Natl. Acad. Sci. U.S.A. 87 (1990) 3526–3529.
[30] K. Kubiak, P.A. Mulheran, Molecular dynamics simulations of hen egg white lysozyme adsorption at a charged solid surface, J. Phys. Chem. B 113 (2009) 12189–12200.
[31] K. Kubiak-Ossowska, P.A. Mulheran, What governs protein adsorption and immobilization at a charged solid surface? Langmuir 26 (2010) 7690–7694.
[32] K. Kubiak-Ossowska, P.A. Mulheran, Mechanism of hen egg white lysozyme adsorption on a charged solid surface, Langmuir 26 (2010) 15954–15965.
[33] G. Raffaini, F. Ganazzoli, Protein adsorption on a hydrophobic surface: a molecular dynamics study of lysozyme on graphite, Langmuir 26 (2010) 5679–5689.
[34] G.A. Voth, Coarse-Graining of Condensed Phase and Biomolecular Systems, CRC Press, Boca Raton, 2009.
[35] V. Tozzini, Multiscale modeling of proteins, Acc. Chem. Res. 43 (2010) 220–230.
[36] V. Tozzini, Coarse-grained models for proteins, Curr. Opin. Struct. Biol. 15 (2005) 144–150.
[37] S.J. Marrink, H.J. Risselada, S. Yefimov, D.P. Tieleman, V.A. de, The MARTINI force field: coarse grained model for biomolecular simulations, J. Phys. Chem. B 111 (2007) 7812–7824.
[38] L. Monticelli, S.K. Kandasamy, X. Periole, R.G. Larson, D.P. Tieleman, S.J. Marrink, The MARTINI coarse-grained force field: extension to proteins, J. Chem. Theory Comput. 4 (2008) 819–834.
[39] C.A. Lopez, A.J. Rzepiela, A.H. De Vries, L. Dijkhuizen, P.H. Hunenberger, S.J. Marrink, Martini coarse-grained force field: extension to carbohydrates, J. Chem. Theory Comput. 5 (2009) 3195–3210.
[40] M.S. Dresselhaus, P. Avouris, Introduction to carbon materials research, Top. Appl. Phys. 80 (2001) 1–9.
[41] G. Hummer, J.C. Rasaiah, J.P. Noworyta, Water conduction through the hydrophobic channel of a carbon nanotube, Nature 414 (2001) 188–190.
[42] L. Zhang, G.F. Zhao, Y. Sun, Effects of ligand density on hydrophobic charge induction chromatography: molecular dynamics simulation, J. Phys. Chem. B 114 (2010) 2203–2211.
[43] H.J. Berendsen, D. Vanderspoel, R. Vandrunen, Gromacs – a message-passing parallel molecular-dynamics implementation, Comput. Phys. Commun. 91 (1995) 43–56.
[44] E. Lindahl, B. Hess, S.D. van, GROMACS 3.0: a package for molecular simulation and trajectory analysis, J. Mol. Model. 7 (2001) 306–317.
[45] R. Sayle, E. Milnerwhite, RASMOL – biomolecular graphics for all, Trends Biochem. Sci. 20 (1995) 374–376.
[46] Z. Guo, D. Thirumalai, Kinetics of protein folding: nucleation mechanism, time scales, and pathways, Biopolymers 36 (1995) 83–102.
[47] A Gautieri, A. Russo, S. Vesentini, A. Redaelli, M.J. Buehler, Coarse-grained model of collagen molecules using an extended martini force field, J. Chem. Theory Comput. 6 (2010) 1210–1218.
[48] R. Diamond, Real-space refinement of the structure of hen egg-white lysozyme, J. Mol. Biol. 82 (1974) 371–391.
[49] R.W. Deitcher, Y. Xiao, C.J. O'Connell, E.J. Fernandez, Protein instability during HIC: evidence of unfolding reversibility, and apparent adsorption strength of disulfide bond-reduced alpha-lactalbumin variants, Biotechnol. Bioeng. 102 (2009) 1416–1427.
[50] Y.Z. Xiao, A.S. Freed, T.T. Jones, K. Makrodimitris, C.J. O'Connell, E.J. Fernandez, Protein instability during HIC: describing the effects of mobile phase conditions on instability and chromatographic retention, Biotechnol. Bioeng. 93 (2006) 1177–1189.
[51] Y.Z. Xiao, T.T. Jones, A.H. Laurent, C.J. O'Connell, T.M. Przybycien, E.J. Fernandez, Protein instability during HIC: hydrogen exchange labeling analysis and a framework for describing mobile and stationary phase effects, Biotechnol. Bioeng. 96 (2007) 80–93.
[52] T.T. Jones, E.J. Fernandez, Hydrophobic interaction chromatography selectivity changes among three stable proteins: conformation does not play a major role, Biotechnol. Bioeng. 87 (2004) 388–399.